Biophysical Journal Volume 65 September 1993 1272–1282

Cytoplasmic Viscosity Near the Cell Plasma Membrane: Measurement by Evanescent Field Frequency-Domain Microfluorimetry

S. Bicknese, N. Periasamy, S. B. Shohet,* and A. S. Verkman

Departments of Medicine and Physiology, Cardiovascular Research Institute, and * Laboratory Medicine; University of California, San Francisco, California 94143-0532 USA

ABSTRACT The purpose of this study was to determine whether the unique physical milieu just beneath the cell plasma membrane influences the rheology of fluid-phase cytoplasm. Cytoplasmic viscosity was evaluated from the picosecond rotation of the small fluorophore 2′,7′-bis-(2-carboxyethyl)-5-carboxyfluorescein (BCECF) by parallel-acquisition Fourier transform microfluorimetry (Fushimi and Verkman, 1991). Information about viscosity within <200 nm of cell plasma membranes was obtained by selective excitation of fluorophores in an evanescent field created by total internal reflection (TIR) of impulse-modulated *s*-plane-polarized laser illumination (488 nm) at a glass-aqueous interface. Measurements of fluorescence lifetime and time-resolved anisotropy were carried out in solutions containing fluorescein or BCECF at known viscosities, and monolayers of BCECF-labeled Swiss 3T3 fibroblasts and Madin-Darby canine kidney (MDCK) cells. Specific concerns associated with time-resolved fluorescence measurements in the evanescent field were examined theoretically and/or experimentally, including variations in lifetime due to fluorophore proximity to the interface, and the use of *s* and *p* polarized excitation. In fluorescein solutions excited with *s*-plane polarized light, there was a 5–10% decrease in fluorescein lifetime with TIR compared to trans (subcritical) illumination, but no change in rotational correlation time (~98 ps/cP). Intracellular BCECF had a single lifetime of 3.7 ± 0.1 ns near the cell plasma membrane. Apparent fluid-phase viscosity near the cell plasma membrane was 1.1 ± 0.2 cP (fibroblast) and 1.0 ± 0.2 cP (MDCK), not significantly different from the viscosity measured in bulk cytoplasm far from the plasma membrane. The results establish the methodology for time-resolved microfluorimetric measurement of polarization in the evanescent field and demonstrate that the cell plasma membrane has little effect on the fluid-phase viscosity of adjacent cytoplasm.

INTRODUCTION

The aqueous compartment of cell cytoplasm consists of a complex array of organized macromolecular structures, including skeletal elements and organelles, and dissolved small (e.g., ions, amino acids, nucleotides) and large (e.g., proteins) solutes (Fulton, 1982; Clegg, 1984; Porter, 1984). The "fluid-phase" cytoplasmic viscosity, defined as the viscosity sensed by a small probe molecule which does not interact with intracellular macromolecular structures, is an important determinant of the kinetics of chemical and enzymatic reactions and solute transport. Recent data indicate that fluid-phase viscosity is an important quantity in the determination of translational diffusion of small polar solutes (Kao et al., 1993). The fluid-phase cytoplasmic viscosity has been estimated by a variety of biophysical techniques, including tracer diffusion, fluorescence photobleaching recovery, electron spin resonance, and steady state fluorescence anisotropy (Lepock et al., 1983; Mastro and Keith, 1984; Luby-Phelps et al., 1986; Dix and Verkman, 1990). Values from ~2 cP to >100 cP (water is 1 cP) have been reported for probe molecules of different sizes and properties. These values provide an upper limit to the fluid-phase viscosity, because they contain additional contributions from probe binding to and collisions with cytoplasmic structures.

We introduced an approach recently to estimate fluid-phase cytoplasmic viscosity from the picosecond rotational motion of small fluorophores dissolved in the cytoplasmic compartment of living cells (Fushimi and Verkman, 1991). Multicomponent analysis of time-resolved anisotropy provided information about the rotation of unbound and bound probe; rotation of unbound probe, which was not influenced by binding and collisional interactions, provided direct information about cytoplasmic viscosity. In fibroblasts and several types of epithelial cells, fluid-phase viscosity was 1.1–1.5 cP, not much higher than that of water (1 cP) (Periasamy et al., 1992). Recent measurements of cytoplasmic viscosity in CV1 and PtK_1 cells by a novel ratiometric method supported the conclusion that fluid-phase viscosity in bulk cytoplasm is similar to that of water (Luby-Phelps et al., 1993). In fibroblasts, fluid-phase viscosity was weakly temperature-dependent (Arrhenius activation energy 3–5 kcal/mol) and nearly independent of cell volume (Fushimi and Verkman, 1991). In MDCK cells grown in isosmotic media, fluid-phase viscosity was near 1 cP, but increased by 40% in response to physiological accumulation of osmolytes upon adaptation to hyperosmolality (Periasamy et al., 1992). The sea urchin egg, a cell thought classically to have a dense cytoplasm, had a higher fluid-phase viscosity of 2.3 cP (Periasamy et al., 1991).

The fluid-phase viscosity is sensitive to the amounts of dissolved organic solutes and the physical state of water. The aqueous compartment just beneath cell membranes provides

Received for publication 2 December 1992 and in final form 11 May 1993.

Address reprint requests to A. S. Verkman at 1065 Health Sciences East Tower, University of California, San Francisco, CA 94143–0532. Tel.: 415-476-2172; Fax: 415-476-3381.

0006-3495/93/09/1272/11 $2.00

a unique physical environment because of the protein-lipid interface, the high concentration of charges and counter ions (required to maintain electroneutrality), and the high density of skeletal protein (Parsegian and Rau, 1984). It has been proposed that the cytoplasm adjacent to cell plasma membranes may have very different solute composition and physical state than "bulk" water, and that localized submembrane signaling mechanisms may exist (Ausiello et al., 1987). Analysis of the physical state of the aqueous compartment adjacent to cell plasma membrane is made difficult by the limited z resolution of widefield or confocal optics (>600 nm).

We report here the application of evanescent field excitation (by total internal reflection) to measure the physical state of cell cytoplasm just beneath the plasma membrane. Time-resolved anisotropy of a small polar fluorophore was measured by frequency-domain microfluorimetry. An important component of this study was the development and validation of methodology for measurement of lifetime and anisotropy decay by excitation of fluorophores in the evanescent field in living cells. The methods were then applied to compare the physical state of membrane-adjacent and bulk water in a nonepithelial (Swiss 3T3 fibroblast) and an epithelial (MDCK) cell type.

METHODS

Cell culture and fluorescence labeling

Swiss 3T3 fibroblasts (CL-101; American type Culture Collection, Rockville, MD) were grown on 18-mm-diameter glass coverslips in DME-H21 medium supplemented with 5% bovine calf serum, 100 units/ml penicillin, and 100 μg/ml streptomycin. Madin-Darby canine kidney (MDCK) cells (passages 54–60, UCSF Cell Culture Facility) were grown in DME medium supplemented with 10% fetal calf serum and antibiotics as above. Cells were maintained at 37°C in a 95% air/5% CO_2 incubator and used 2–4 days after plating. Cells were loaded with 2′,7′-bis-(2-carboxyethyl)-5-carboxyfluorescein, acetoxymethyl ester (BCECF-AM) by a 10-min incubation with 10 μM BCECF-AM (Molecular Probes, Junction City, OR) in the culture medium. Cells were washed and bathed in Hanks' balanced salt solution (HBSS) after loading.

Instrumentation

An instrument schematic is shown in Fig. 1. The output of a 4-watt argon ion laser (488 nm) was attenuated and impulse-modulated at a 5-MHz repetition rate using a Pockels cell. The modulated beam was initially polarized along the z axis. A fraction of the beam (~5%) was split by a quartz coverslip for a reference signal (PMT 2). After reflections by two mirrors (mounted on two-axis micropositioners) the beam was polarized along the y axis. The beam was steered onto the sample through a cubic glass prism to give an s-polarized configuration. No dichroic mirror was used. In some experiments, the polarization of the excitation beam was rotated by 90° using a 488-nm λ/2-quartz plate (Melles-Griot) to give p-polarized excitation. Incident angles were calculated from the geometry of the optical configuration. Refractive indices of the prism ($n_{488\ nm}$ = 1.522) and coverslip ($n_{488\ nm}$ = 1.530) were used to calculate the incident angle at the glass:water interface. The unfocused laser beam produced an elliptical spot (1.5-mm wide × 3-mm long) in the sample plane. In some experiments, the excitation beam was focused by a lens (40-cm focal length) to produce a 0.6-mm-wide × 1-mm-long spot. The sample and prism were positioned on the x, y translation stage of a Nikon inverted microscope.

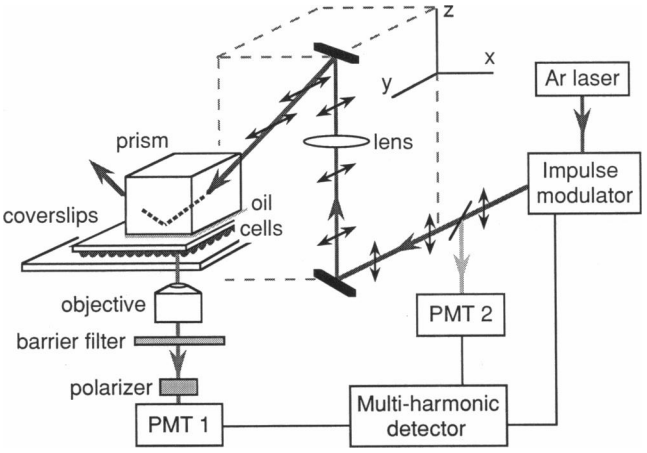

FIGURE 1 Schematic of apparatus for time-resolved TIR microfluorimetry. The beam produced by an argon laser is modulated by a Pockels cell and split to provide a reference beam at photomultiplier, PMT 2. The beam is directed to the cell sample through a cubic glass prism at a specified angle of incidence. Emitted fluorescence passes through the microscope objective, barrier filter, and analyzing polarizer to photomultiplier, PMT 1. Phase and modulation data are obtained by multifrequency cross-correlation detection. See text for details.

Cells (facing downward) were "sandwiched" between the coverslip on which they were grown and a second larger coverslip. A 140-μm thick layer of HBSS was maintained between the coverslips by spacers. Optical contact between the glass TIR prism (BK-7 type glass, refractive index $n_{589\ nm}$ = 1.517) and the coverslip was made with immersion oil ($n_{589\ nm}$ = 1.518). In some experiments, the TIR prism was removed for direct ("trans") sample excitation, or the incident beam was directed along the optical axis of the microscope for conventional epi-illumination (Verkman et al., 1991). Sample fluorescence was collected by an objective lens (Leitz 40 ×, 0.65 N.A. quartz-glycerol; or Leitz 25 ×, 0.35 N.A. glass-air), passed through a barrier filter (Schott glass OG 515) and Glan-Thompson calcite-analyzing polarizer, and detected by a photomultiplier (PMT 1, Hamamatsu R3896). The analyzing polarizer could be rotated by 90°. For s-polarized excitation, the polarizer was rotated between parallel (y axis) and perpendicular (x axis) orientations for measurement of anisotropy decay; the polarizer was set to the "magic" angle (54.7° from the y axis) for measurement of lifetime. Depolarization of emitted fluorescence by the objectives used in this study was insignificant as confirmed by the independence of time-resolved anisotropy measured using the N.A. 0.65 and 0.35 objectives.

The multiharmonic detector shown in Fig. 1 consisted of components of a Fourier transform fluorimeter (48000 MHF, SLM Instruments Inc., Urbana, IL). A low frequency (7.29 Hz) replica of the nanosecond time-domain signal was obtained by parallel cross-correlation detection for direct analog-to-digital conversion and fast Fourier transform to the frequency-domain (Periasamy et al., 1991). Analysis of lifetime and time-resolved anisotropy were performed by a comparative approach. Generally four to five pairs of measurements (each acquisition, 3–10 s) were obtained, comparing sample and reference (fluorescein in 0.1 N NaOH, lifetime 4.0 ns) for measurement of lifetime, and parallel and perpendicular orientations of the analyzing polarizer for measurement of anisotropy decay. The phase-modulation data consisted of phase angles and modulation ratios at 40 discrete, equally spaced modulation frequencies (5–200 MHz). Other details of the data acquisition and analysis routines were described previously (Verkman et al., 1991). Anisotropy decay measurements required the inclusion of a geometric factor (generally ~1.05) to correct for the differential detection of parallel versus perpendicular emission polarization (Fushimi et al., 1990). The geometric factor was determined using a dilute solution of fluorescein in 0.1 N NaOH which has a single rotational correlation time of 110 ps. Modulation ratio values at each frequency were divided by the geometric factor. Median phase and modulation values for paired data were analyzed

by nonlinear least-squares for determination of lifetimes and rotational correlation times (Periasamy et al., 1991). Time-resolved anisotropy, $r(t)$, in cells was described by two rotational correlation times (τ_{1c} and τ_{2c}) and a fractional anisotropy loss (f_1), as given by $r(t) = r_0[f_1 e^{-t/\tau_{1c}} + (1 - f_1)e^{-t/\tau_{2c}}]$ where r_0 is the anisotropy in the absence of depolarizing rotations (0.392 for BCECF).

Image analysis

To record cell images, the photomultiplier was replaced by a silicon-intensified target camera (SIT66; Dage-MTI Inc., Michigan City, IN) operated at fixed gain. Fluorescence was collected by a 40 × objective (Nikon, 0.55 N.A., long working distance). Eight-bit, 512 × 512-pixel images were digitized by a frame grabber (DT2861; Data Translation, Marlboro, MA) and numerical processing board (DT2858) in an 80486 PC computer. Gain and zero offset were adjusted to maintain pixel intensities in the linear response range of the camera. Images were hard-copied by a Seikosha VP1500 video printer (Seikosha America Inc., Mahwah, NJ).

RESULTS

Lifetime determination in the evanescent field

In the experimental measurements reported here, an evanescent field is produced by total internal reflection (TIR) at a dielectric (glass, $n_{488\,nm} = 1.530$) interface to excite fluorophores in an aqueous environment ($n_{488\,nm} = 1.337$) beyond the interface. Certain unique properties of the evanescent field influence time-resolved fluorescence measurements made by TIR illumination. Drexhage (1970) reported that fluorophore proximity to a dielectric interface influences the decay time. This phenomenon, here referred to as "far-field effect," arises from constructive and destructive interference between direct fluorescence and fluorescence reflected from the dielectric interface. This far-field effect gives rise to a dependence of fluorescence intensity on fluorophore distance, z, from the interface, causing variations in dissipated power (with corresponding inverse variations in fluorescence lifetime). For a fluorophore very close to an interface, ($z \ll$ emission wavelength), power dissipation is subject to a second phenomenon called the "near-field effect" (Hellen and Axelrod, 1987; Lukosz and Kunz, 1977; Chance et al., 1978). An excited fluorophore emits an evanescent field with an amplitude that decays exponentially with distance from the fluorophore. If the field extends to an interface having a more optically dense medium (higher refractive index), it is transmitted as a plane-propagating wave into the denser medium at supercritical angles (Born and Wolf, 1970). This additional power dissipation into the denser medium varies inversely with fluorophore distance from the interface and shortens the fluorescence lifetime.

Near and far field effects are combined to calculate power dissipation ($P_x(z), P_y(z), P_z(z)$) from excited dipoles oriented along the x, y, or z axes with the interface in the x, y plane (see Appendix; Eqs. A1–A3, Fig. 6 and Fig. 2 *A*). In Fig. 2 *A*, dissipated power for fluorescein (emission $\lambda = 531$ nm) at a distance, z, from a glass:water interface is shown relative to dissipated power in the absence of the dielectric. The "near-field effect" has the dominant impact on power dissipation (and fluorescence lifetime) very close to the interface ($z < 0.1$ μm). Fig. 2 *A* thus shows that power dissipation varies with both z position and dipole orientation relative to the interface.

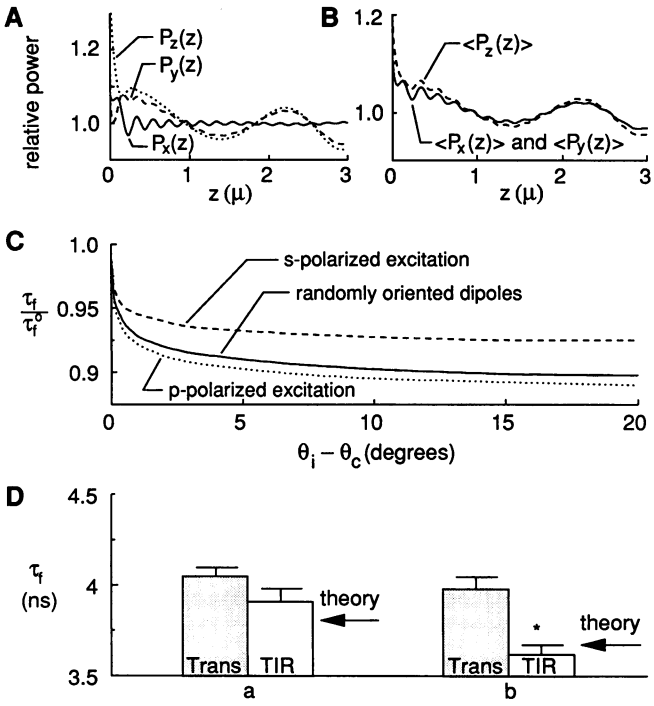

FIGURE 2 Fluorescence lifetime decay near a glass-aqueous interface. (*A*) Ratio of radiated power for a fluorophore positioned at a distance z beyond a glass ($n = 1.530$):water ($n = 1.337$) interface to that of the same fluorophore in the absence of an interface. Relative power was calculated by Eqs. A1–A3. $P_x(z)$, $P_y(z)$, and $P_z(z)$ designate the relative power dissipated from fluorophores oriented along the x, y, or z axis (see Fig. 6). (*B*) Ratio of power dissipation for an ensemble of randomly oriented fluorophores at a distance, z, beyond a glass:water interface to those in the absence of an interface when excited by light polarized along the x, y, or z axes. Relative power was calculated by Eqs. A4–A6 (see Results and Appendix). (*C*) Ratio of fluorescence lifetime by TIR evanescent field excitation to lifetime by trans (subcritical) excitation, τ_f/τ_f^0, as a function of incident angle, θ_i (where θ_c is the critical angle = 60.9°). Incident light was *s*-polarized (along the y axis) or *p*-polarized (combination of polarization along the x and z axes, see text). τ_f/τ_f^0 was calculated from the results of Eqs. A7–A10. τ_f/τ_f^0 for randomly oriented dipoles was calculated from Eqs. A7 and A8 without photoselection (see Appendix). (*D*) Fluorescence lifetimes (mean ± SE) measured in aqueous solutions of 140 μM fluorescein at (*a*) 0.5° ($n = 3$) and (*b*) 2° ($n = 3$) beyond the critical angle by TIR excitation. The arrows indicate the lifetimes predicted by the theory for randomly oriented dipoles.

To calculate the power dissipation for an ensemble of randomly oriented dipoles excited by an *s*- or *p*-plane-polarized evanescent field, the power dissipation functions $P_x(z)$, $P_y(z)$, and $P_z(z)$ must be modified to incorporate three additional considerations: (*a*) the contribution to total power dissipation by dipoles oriented parallel and perpendicular to the interface, (*b*) the photoselection of randomly oriented dipoles by the polarized evanescent field, and (*c*) the decay of the evanescent field intensity with distance, z, from the interface (see Appendix). The three factors can be considered independently. (*a*) For a glass:water interface, where the ratio of power dissipation by parallel (x, y) dipoles to that of

perpendicular (z) dipoles is ~1, total power is described approximately by $P_T(z) = [P_z(z)] \cos^2\psi + [P_x(z) + P_y(z)] \sin^2\psi$ (Hellen and Axelrod, 1987), where ψ is the polar angle of the emission dipole measured from the z axis. (b) The angular density of photoselection among randomly oriented dipoles by a polarized excitation field ($|\mu \cdot E_{ex}|$) is described by $\cos^2\psi \sin\psi$ for s-polarized excitation and $\sin^2\psi \sin^2\phi \cos\phi$ for p-polarized excitation, where ψ and ϕ are the polar and azimuthal angles. (c) The TIR evanescent field intensity, I, is described by

$$I = I_0(\theta_i)e^{-z/d(\theta_i)}, \tag{1}$$

where I_0 is the initial evanescent intensity as a function of the incident angle, θ_i (Eqs. A11–A13). The decline of intensity in the evanescent field is thus an exponential function of the distance, z, from the interface with characteristic penetration depth, d, given by

$$d(\theta_i) = [\lambda_0/4\pi](n_1^2\sin^2\theta_i - n_2^2)^{-1/2}, \tag{2}$$

where n_1 and n_2 are the refractive indices of glass and water, and θ_i is the incident angle of the light with vacuum wavelength λ_0. Considerations a, b, and c are incorporated to calculate lifetime by integration of the power, photoselection, and evanescent field functions over the angles ψ and ϕ and the distance variable, z, as given by

$$N(\omega,\theta_i) = \int_0^\infty dz \int_0^{\pi/2} d\phi \int_0^{\pi/2} \sin\psi\, d\psi \tag{3a}$$

$$\cdot \frac{|\mu \cdot E_{ex}|^2 I_0 e^{-z/d(\theta_i)} \omega[1/\{P_z(z)\cos^2\psi + [P_x(z) + P_y(z)]\sin^2\psi\}]^2}{1 + \omega^2[1/\{P_z(z)\cos^2\psi + [P_x(z) + P_y(z)]\sin^2\psi\}]^2}$$

$$D(\omega,\theta_i) = \int_0^\infty dz \int_0^{\pi/2} d\phi \int_0^{\pi/2} \sin\psi\, d\psi \tag{3b}$$

$$\cdot \frac{|\mu \cdot E_{ex}|^2 I_0 e^{-z/d(\theta_i)}[1/\{P_z(z)\cos^2\psi + [P_x(z) + P_y(z)]\sin^2\psi\}]}{1 + \omega^2[1/\{P_z(z)\cos^2\psi + [P_x(z) + P_y(z)]\sin^2\psi\}]^2}$$

where ω is the modulation frequency for frequency-domain lifetime measurement. $N(\omega,\theta_i)$ and $D(\omega,\theta_i)$ are used to calculate phase angles $\{\phi = \tan^{-1}[N(\omega,\theta_i)/D(\omega,\theta_i)]\}$ and modulation ratios $\{m = [D(\omega,\theta_i)^2 + N(\omega,\theta_i)^2]^{1/2}\}$ (Weber, 1981). The details of the calculation of $N(\omega,\theta_i)$ and $D(\omega,\theta_i)$ for photoselected and randomized fluorophores are provided in the Appendix (Eqs. A4–A14).

TIR excitation produces a distribution of fluorescence lifetimes (inverse of power dissipation), because lifetimes vary with fluorophore distance from and orientation to the interface (see Fig. 2 A). Evanescent field penetration decreases with increasing θ_i (Eq. 1); therefore, the ensemble of excited fluorophores shifts toward the interface with increasing θ_i and is subject to near-field effects (which shorten fluorescence lifetime). For a homogeneous distribution of fluorophores excited by TIR, the term $[I_0 e^{-z/d(\theta_i)}]$ in Eqs. 3a and 3b weights the contribution of each lifetime in the lifetime distribution. For example, dipoles within 1 μm of a glass:water interface (n = 1.53:1.33) with random orientation at the time of emission have relative lifetimes that vary from 0.859 to 1.006 (relative to lifetime without the interface). Mean lifetimes of these dipoles are 0.94, 0.92, and 0.91 for θ_i at 1, 5, and 10° beyond the critical angle. Standard deviations of these lifetime distributions are 0.04, 0.05, and 0.06, respectively.

Apparent average lifetimes, $\tau_f(\theta_i)$, were determined by fitting a single component model to ϕ and m values (40 values for ω = 5–200 MHz) calculated from $N(\omega,\theta_i)$ and $D(\omega,\theta_i)$. In Fig. 2 C, $\tau_f(\theta_i)$ for TIR illumination is shown relative to τ_f^0 (fluorescence lifetime with no dielectric interface) for incident angles (θ_i) greater than the critical angle (θ_c). At a given incident angle, θ_i, fluorescence lifetime is shorter for p-polarized TIR excitation of fixed fluorophores due to its photoselection of z-oriented dipoles with higher power dissipation (see Fig. 2 A). Fluorophores that randomize their orientation at the time of emission have $\tau_f(\theta_i)/\tau_f^0$ values between those for fixed dipoles photoselected by s- or p-polarized excitation (see Fig. 2 C). $\tau_f(\theta_i)/\tau_f^0$ values given in Fig. 2 C were calculated for a quantum yield, Q_y, of unity. Because near- and far-field effects do not influence nonradiative decay rates, lifetimes are less sensitive to the dielectric interface when $Q_y < 1$. $\tau_f(\theta_i)/\tau_f^0$ is given as Q_y/P_r, where P_r is the ratio of radiated power dissipation for fluorophores with and without a nearby dielectric interface (Hellen and Axelrod, 1987).

In Fig. 2 D, lifetimes measured with TIR excitation are slightly shorter than lifetimes measured with trans excitation. At 2° beyond the critical angle, the difference is significant ($P < 0.05$). As predicted, the higher incident angle of excitation (θ_i) and reduced field penetration produced a greater reduction in the lifetime.

Measurements in aqueous solution

The TIR condition was confirmed by using a thin film (10 nm) of a lipophilic carbocyanine dye (1,1′-dioctadecyl-3,3,3′,3′-tetramethylindocarbocyanine perchlorate; di-I-C18:3) deposited on the glass coverslip (Axelrod, 1981). Film thickness was confirmed by absorption measurement. The dye film was in the position of the cells as shown in Fig. 1, and the solution layer between the coverslips contained 20 μM fluorescein in HBSS (titrated to pH 8.0). For subcritical angles of incidence at the coverslip-water interface (<60.9°), the fluorescence was predominantly that of fluorescein (green) from the 140-μm thick fluorescein solution. For supercritical angles of incidence, the fluorescence was predominantly that of the carbocyanine dye (red).

Measurements were carried out on aqueous solutions of fluorescein of known refractive index and viscosity. The experimental configuration was as shown in Fig. 1 (without the cells) in which the fluorescein solution was maintained in the 140-μm aqueous layer. Fig. 3 shows representative phase-modulation plots for analysis of lifetime and anisotropy decay obtained for trans (prism absent) and TIR (prism present) excitation of fluorescein in HBSS (pH 8.0) containing 0, 26,

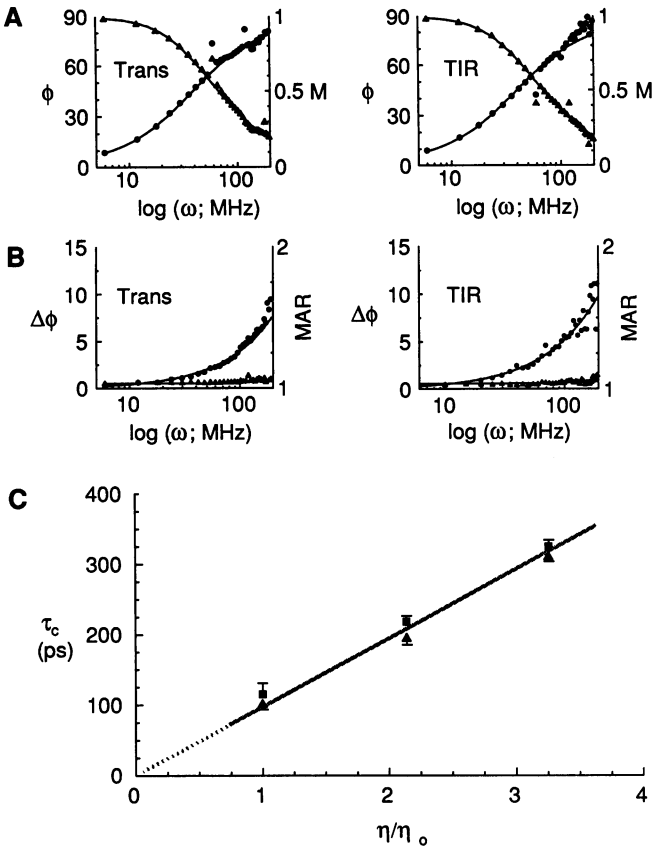

FIGURE 3 Lifetime and time-resolved anisotropy of fluorescein measured by TIR and trans excitation. Measurements were carried out at θ_i = 62–66° using *s*-plane polarized light. (*A*) Representative experiments showing phase angles, ϕ (*circles*) and modulation factors, M (*triangles*), with single component lifetime fit. (*B*) Representative anisotropy measurements showing differential phase angles, $\Delta\phi$ (*circles*) and modulation amplitude ratios, MAR (*triangles*), with single rotational correlation time fit. (*C*) Rotational correlation times (τ_c, mean ± SE, n = 15–26) for 140 μM fluorescein in HBSS (titrated to pH 8.0), containing 0, 26 and 38% glycerol. τ_c measured by trans (*triangles*) and TIR (*squares*) excitation are shown as a function of the ratio of sample to water viscosity, η/η_0. The least-squares fitted line has a slope of 98 ± 2 ps/cP.

and 38% glycerol in water. The reference solution for lifetime determination was fluorescein in 0.1 N NaOH measured by trans excitation. Phase-modulation data for trans and TIR excitation (Fig. 3 *A*) were fitted well by a single component lifetime model. There was no difference in lifetimes for fluorescein in water or in glycerol/water mixtures (but there was a difference between lifetimes measured by trans and TIR excitation as predicted by theory as in Fig. 2 *D*, see above). Lifetimes measured by trans illumination were not different from those measured by epi-illumination (not shown).

Fig. 3 *B* shows phase-modulation data for anisotropy measurements made with *s*-polarized trans and TIR excitation. The time-resolved anisotropy data were described well by a single isotropic rotator model, $r(t) = r_0 e^{-t/\tau_c}$. Fig. 3 *C* shows the fitted rotational correlation times, τ_c, for *s*-polarized trans and TIR excitation. Rotational correlation times were not significantly different for *s*-polarized TIR excitation compared to trans excitation (or epi-illumination, not shown). *p*-polarized excitation could not be used for anisotropy decay measurements because the fluorescence emission was depolarized for the experimental geometry used here. As predicted by the Stokes-Einstein relation, τ_c increased linearly with solution viscosity. These results validate the measurement of time-resolved anisotropy by an *s*-polarized evanescent field.

Measurements in cultured cells

TIR excitation in cells was confirmed by imaging Swiss 3T3 fibroblasts and MDCK cells. Fig. 4, *A* and *C*, show Swiss 3T3 fibroblasts and MDCK cells imaged by trans excitation. The entire cell was illuminated and the maximum fluorescence intensity appeared at the center of the cell where cell depth is greatest. In Fig. 4, *B* and *D*, cells were imaged with *s*-polarized TIR excitation. In these experiments, 90% of fluorophore excitation occurs within <200 nm of the glass coverslip and fluorescence intensity is greatest where the cell has close contact with the glass substrate. The 3T3 cells show a "footprint" that appears to coincide with their periphery, while the MDCK cells appear to have fairly equal contact at all points. Additional information about the contact geometry was obtained by imaging unlabeled 3T3 fibroblasts bathed in an aqueous solution of fluorescein-dextran (2000 kDa, 2 mg/ml). This large dextran was excluded from the cells and the space between the cells and the glass substrate. Fig. 4 *E* (trans excitation) shows uniform strong fluorescence, because the 140-μm aqueous layer (containing fluorescein-dextran) is much greater than the thickness of the nonfluorescent cell (<2 μm). With TIR excitation, the depth of the evanescent field (<200 nm) does not extend beyond the cells (Fig. 4 *F*), so that fluorescence is absent in areas where the cells have excluded fluorophore (producing "silhouette" images).

Fig. 5 shows representative phase-modulation data for analysis of lifetime (Fig. 5 *A*) and anisotropy decay (Fig. 5 *B*) obtained for trans and TIR excitation of BCECF in cells. Fig. 5 *C* shows average lifetimes, τ_f, for BCECF in aqueous solution and in cells. No significant difference was observed for BCECF lifetime, τ_f, with trans or TIR excitation in cells. The slightly longer lifetime for BCECF in cells than in aqueous solution may be related to differences in the intracellular versus external environment (Chen and Scott, 1985). Anisotropy analysis was performed using a model containing two correlation times (see Methods). Fig. 5 *C* also shows the shorter correlation times, τ_{1c}, corresponding to rotation of unbound BCECF (fractional amplitude, f_1 = 70–85%). Correlation times, τ_{2c}, for the remaining (and assumed bound) fluorophores ranged from 10 to 25 ns. Rotational correlation times obtained by trans and TIR excitation of BCECF in cells were not significantly different, giving average fluid-phase viscosities of 1.1 ± 0.2 cP (3T3 fibroblasts) and 1.0 ± 0.2 cP (MDCK cells). Therefore, fluid-phase viscosity is not different in bulk cytoplasm and cytoplasm very near the cell plasma membrane.

DISCUSSION

We have validated an approach to measure fluorescence lifetime decay and time-resolved anisotropy in an evanescent

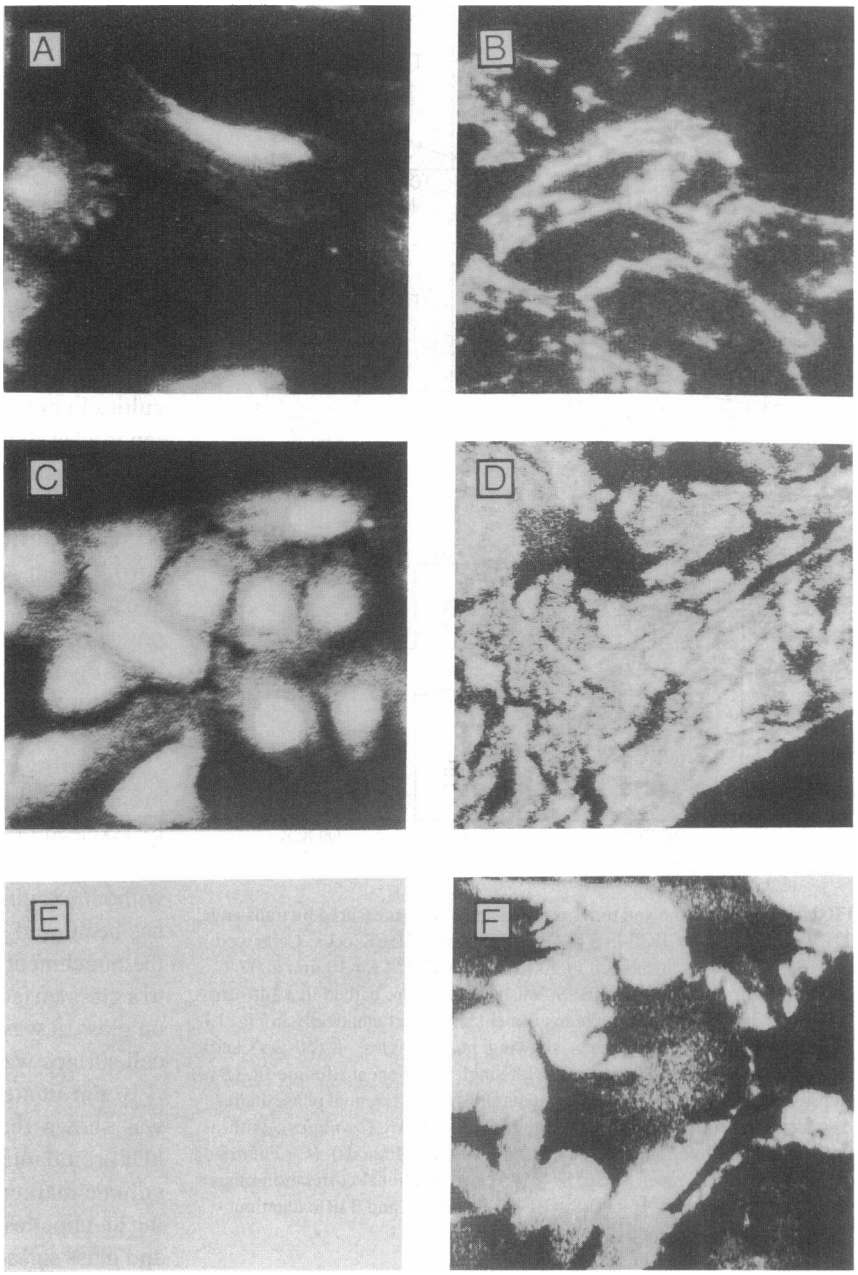

FIGURE 4 Photomicrographs of Swiss 3T3 fibroblasts and MDCK cells with trans (*left*) and TIR (*right*) excitation. Swiss 3T3 fibroblasts (*A* and *B*) and MDCK cells (*C* and *D*) were incubated with 10 μM BCECF-AM for 10 min at 37°C and then washed. Trans illumination (*left*) shows regions of greatest cell thickness, whereas TIR illumination (*right*) shows regions of closest contact between the cell and coverslip. Swiss 3T3 fibroblasts (*E* and *F*) were imaged after immersion in HBSS (pH 8.0) containing fluorescein-dextran (2000 kDa, 2 mg/ml). Trans excitation (*E*) produced evenly distributed fluorescence across the entire visual field, whereas TIR excitation (*F*) revealed dark areas where the fluorophore was excluded by the overlying cells.

field at a glass-aqueous interface by frequency-domain microfluorimetry. Fluid-phase viscosity within <200 nm of the plasma membrane in Swiss 3T3 fibroblasts and MDCK cells was found to be essentially the same as that in bulk cytoplasm and very close to that of water. TIR fluorescence spectroscopy provides a unique method to probe the properties of membrane-associated and aqueous-phase components adjacent to a cell plasma membrane. The ability to control the penetration depth from the interface of evanescent field excitation makes this method uniquely suited for the study of cell structures and properties that vary with distance from the substrate on which they are grown.

The limited penetration and defined polarization of TIR fluorescence excitation has been used to study a number of phenomena, including binding of fluorophores to a surface, and orientation mobility of fluorophores in thin films. Hlady (1991) exploited the shallow penetration of TIR illumination to image the binding of fluorescein isocyanate (FITC)-IgG at interfaces having different hybrophobicities. Leibman et al. (1991) used two simultaneous TIR beams at different incident angles (giving different penetration depths) to obtain real-time dynamic measurements of IgG binding to plasminogen activator protein immobilized at an interface. Binding kinetics were derived from the rate of change in fluorescence intensity, and the distance of bound fluorophores from the interface was calculated from the ratio of fluorescence intensities produced by the two beams. Fluorescence recovery after photobleaching (FRAP) by TIR illumination allows investigation of translational and rotational mobility of molecules that interact with surfaces. Tilton et al. (1990) used TIR to investigate the translational mobility of BSA adsorbed onto a poly(methylmethacrylate) surface. Timbs

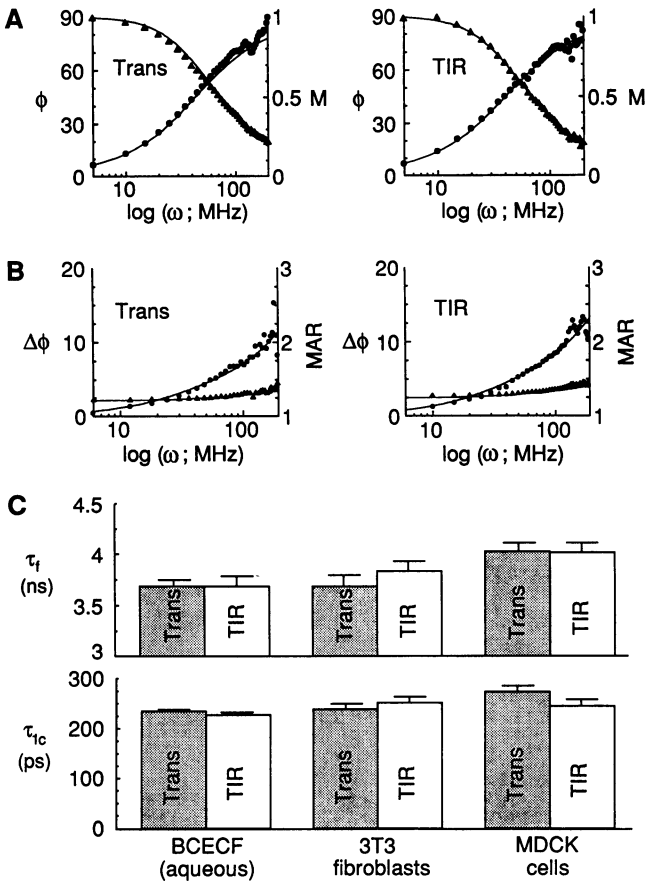

FIGURE 5 Lifetime and time-resolved anisotropy measured by trans and TIR excitation of BCECF in 3T3 fibroblasts and MDCK cells. Cells were grown for 2–4 days, incubated in 10 μM BCECF-AM for 10 min at 37°C, and washed four times with HBSS. Washed cells were bathed in a 140-μm layer of HBSS and placed in the instrument shown schematically in Fig. 1. (*A*) Representative experiments showing phase angles, ϕ (*circles*) and modulation factors, M (*triangles*), with single component lifetime fit. (*B*) Representative anisotropy measurements showing differential phase angles, $\Delta\phi$ (*circles*) and modulation amplitude ratios, MAR (*triangles*), with a two-component rotational correlation time fit (see Methods). (*C*) Fluorescence lifetimes (τ_f, mean ± SE, n = 2–6), and rotational correlation times (τ_{1c}, mean ± SE, n = 16–34) for BCECF by trans and TIR excitation.

and Thompson (1990) measured the rotational mobility of antibodies and lipids in a phospholipid monolayer at the TIR interface by TIR-polarized photobleaching recovery. Photoselection by the polarized evanescent field has been used to investigate the orientation of fluorophores near the TIR interface. Thompson et al. (1984) determined the orientational distribution of labeled phospholipids in a lipid monolayer deposited at the TIR interface by TIR polarization.

Time-resolved fluorimetry has been used extensively for measurement of fluorescence lifetimes in bulk solution, and more recently in single cells by epifluorescence microscopy (Verkman, 1991). TIR excitation makes possible the measurement of time-resolved fluorescence of fluorophores near a TIR interface. Masuhara et al. (1986) made time-domain lifetime measurements of POPOP and *N*-ethycarbazole in thin polystyrene films at a TIR interface. Possible experimental difficulties were investigated, including changes in polarization in the evanescent field because of birefringence of the TIR optics (sapphire prism), and changes in the refractive index in the sample layers containing fluorophores. Fluorophore lifetimes were obtained and the fractional contribution of each lifetime provided a measure of the relative concentration of each fluorophore. Suci and Hlady (1990) used TIR illumination to obtain time-resolved phase-modulation measurements of Texas-Red-labeled bovine serum albumin in solution and adsorbed at a TIR interface. Differences in fluorescence lifetime components were reported for fluorophores in bulk solution and adsorbed states, despite high values ($\gg$1) of χ^2 which indicate some difficulties in modeling the data. A longer lifetime (~4.2 ns) was reported as the major component for fluorophores in the bulk solution, whereas a shorter lifetime (~0.6 ns) was reported as the major component for fluorophores in the adsorbed state. This difference was attributed to quenching effects occurring with adsorption. The "near-field" effect described above (see Results) was not considered, but may be an important factor responsible for the decreased fluorescence lifetimes measured for the adsorbed fluorophore. Time-resolved anisotropy has not been measured previously by evanescent field excitation.

The utility of TIR fluorimetry for the investigation of the properties of plasma membranes in living cells was proposed by Axelrod (1981). It was shown that cell-substrate contact and structure in submembrane cytoplasm could be studied without exciting fluorescence deeper in the cytoplasm. TIR has been used subsequently in studies of the morphology of the attachment points (and aqueous gaps) of cells adherent to a glass surface (Gingell et al., 1985). In fibroblasts cultured on glass, it was estimated that the gap between the glass and cell surface was 50–100 nm in areas of "close contact," and ~10 nm in areas of "focal contact" (Lanni et al., 1985). It was shown that a small volume marker (FITC-dextran, 4 kDa) could intercalate in the contact regions, whereas a large volume marker (FITC-dextran, 157 kDa) could not, providing an upper estimate of 150 nm for the gap between the cell and glass surface (Gingell et al., 1985). It is clear from these studies that the optical model for the cell-substrate interface must consist of serial layers with different thicknesses and refractive indices. In addition, the aqueous gap between the cell membrane and substrate reduces the penetration of the evanescent field beyond the membrane and into the cell. The viscosities measured here include cytoplasm within <200 nm beneath the membrane at maximum, and may include only ~50 nm of cell cytoplasm just below the membrane with large aqueous gaps reported by Gingell et al. (1985).

The multilayer model appropriate for quantitative applications of evanescent field-excited fluorescence near the cell membrane consists of four layers (Reichert and Truskey, 1980; Lanni et al., 1985; Gingell et al., 1987): the thick glass substrate of refractive index n_1 = 1.53 (layer 1), the culture medium of refractive index n_2 ~1.33 of 10–100-nm thickness (layer 2), the plasma membrane of refractive index n_3 ~1.40 of 4-nm thickness (layer 3), and the cytoplasm of

index n_4 ~1.37 of 1–10 μm thickness (layer 4). The possibility exists for the generation of a propagating wave confined to the cell plasma membrane (eventually scattered out if not absorbed) at incident angles between $\sin^{-1}(n_4/n_1) = 63.6°$ and $\sin^{-1}(n_3/n_1) = 66.2°$. This complication was avoided by performing all cell TIR experiments at angles > 66.2° to ensure the production of an evanescent field in all layers including the cell cytoplasm. Under these conditions, the cytoplasmic layer can be treated as infinitely thick compared to the penetration of the evanescent field. Penetration of the evanescent field into the cell cytoplasm is slightly increased by the higher refractive index of the interposed membrane layer ($n_3 = 1.4$), but the change is insignificant because of the very small thickness of the membrane.

Because absorption probabilities are identical for evanescent field photons and photons of normally propagating plane waves (Carniglia et al., 1972), evanescent field excitation is suitable for many fluorescence techniques. However, there are some specific concerns for time-resolved measurements made by evanescent field excitation. *p*-Polarized incident light (see Appendix figure) produces an evanescent field that is elliptically polarized with a polarization vector that "cartwheels" along its direction of propagation (Axelrod et al., 1984; Axelrod, 1989). Therefore, time-resolved anisotropy measurements require careful alignment of the incident beam to give *s* polarization, producing linear *s* polarization in the evanescent field. Materials used in the prisms and coverslips must be free of birefringence that would alter the polarization of the evanescent field. Another concern is that the fluorescence lifetime of a fluorophore near a dielectric interface is different than that far from an interface. As described in the Results and Appendix, this complex phenomenon depends on fluorophore orientation, excitation polarization, and evanescent field penetration depth. For a fluorophore with quantum yield of unity, the theory predicts a maximum ~10% decrease in fluorescence lifetime for fluorophores in an aqueous environment very near a glass interface (see Fig. 2 *C*). Interestingly, we found that lifetimes of BCECF in cells were not measurably affected by TIR excitation, unlike those measured in aqueous solutions (see Fig. 5 *C*). One possible explanation is that fluorophores in the aqueous compartment of cell cytosol cannot approach the dielectric interface closer than the ~4-nm width of the plasma membrane and may be kept much farther away (~50–100 nm) by membrane-associated macromolecules and the aqueous space between the cell plasma membrane and the glass substrate (Lanni et al., 1985) (see Fig. 4). Only those fluorophores that are very close ($z < 100$ nm) to the interface have significantly increased power dissipation that reduces observed fluorescence lifetime (see Fig 2 *B*). Fluorophore interactions with cytoplasmic components are more likely to produce significant changes in fluorescence lifetime than is proximity to the dielectric interface (Chen and Scott, 1985); thus, changes in fluorescence lifetime associated with evanescent field excitation should not be a serious concern for time-resolved TIR measurements in cells.

The principal biological conclusion of this study is that fluid-phase viscosity in cytoplasm adjacent to the plasma membrane is similar to that of water, and not different from that of bulk cytoplasm. This result does not support the proposal that membrane-adjacent cytoplasm contains significant amounts of "organized water" or "gel-like cytoplasm" resulting from adjacent membrane lipids and proteins, and cytoplasmic skeletal proteins. Assuming an average gap of 25 nm between the coverslip and the cell membrane, a bilayer thickness of 4 nm, and an exponential distance constant (*d*, Eq. 2) of 80 nm for a glass-aqueous interface, the viscosity information was obtained in this study at an average distance of 50 nm from the inner bilayer surface. If a region of membrane-adjacent cytoplasm had much higher viscosity (e.g., 10 cP), then the statistical confidence of our results would suggest that the thickness of this viscous layer should be <4 nm, equivalent to a layer of ~12 water molecules. It must be recognized that it is not possible to probe solute-excluded volumes by the fluorescence methods described here; however, the relative uniformity of TIR emission suggests that little if any such volumes are present. A detailed analysis of the distribution of fluorophores in the evanescent field will require deconvolution of images obtained at a series of illumination angles (equivalent to a series of *d* values) (Thompson and Burghardt, 1986).

The determination of fluid-phase viscosity in membrane-adjacent cytoplasm is an important initial step is defining the factors that hinder diffusion of small and large solutes. Kao et al. (1993) reported that translational diffusion of a small polar solute in bulk cytosol was three to four times slower than that in water, and modeled the hindrance to diffusion in term of three independent factors: increased fluid-phase viscosity, solute binding to intracellular structures, and solute collisions with intracellular structures. A similar approach should apply to the analysis of solute translation in membrane-adjacent cytoplasm, with the added complexities that diffusion may be anisotropic because of extended skeletal structures, and may vary with distance from the bilayer. In addition, the presence of skeletal attachments may impede the motion of larger solutes (by sieving) to a greater extent near the membrane than in bulk cytoplasm. Analysis of these factors will require microsecond photobleaching measurements using TIR illumination.

APPENDIX

The purpose of this appendix is to calculate the effect of a dielectric interface on the lifetime of fluorophores near the interface as modeled by a constant-amplitude dipole. Excitation and power dissipation of dipoles is dependent upon their orientation relative to the polarization vector of the evanescent field and glass-aqueous TIR interface, as well as the distance from the interface. Fig. 6 shows the optics geometry, where the *s*- or *p*-polarized beam impinges on the glass-aqueous interface with incident angle, θ_i. Total internal reflection produces an evanescent field in the aqueous environment

with s polarization (electric vector parallel to the y axis) or p polarization (electric vector having components along the x and z axes). The polar and azimuthal angles between the emission dipole and z axis are ψ and ϕ, respectively.

Eqs. A1–A3 give the total dissipated power, $P_x(z)$, $P_y(z)$, and $P_z(z)$, for an excited dipole with orientation along the x, y, or z axes (Hellen and Axelrod, 1987). Here z is the dipole distance from the interface, v is the sine of the incident angle of emitted plane wave with the glass-aqueous interface, k_2 is the magnitude of the wave vector for the emitted light, ϵ_2 is the dielectric constant of the dipole environment, r^s and r^p are Fresnel reflection coefficients of the glass:water interface for s- and p-polarized plane waves, and μ is the transition dipole moment. k_2, ϵ_2, and μ were taken as unity for calculation of relative power dissipation. The Fresnel coefficients are functions of the incident angle of the plane wave with the interface (Hellen and Axelrod, 1987).

$$P_x(z) = \frac{ck_2^4}{2\epsilon_2^{3/2}} Re\left[\int_0^\infty dv v(1 - v^2)^{1/2} \times \left(\frac{\mu^2}{2} \{1 + r^s \exp[i2k_2 z(1 - v^2)^{1/2}]\} \right) \right] \quad \text{(A1)}$$

$$P_y(z) = \frac{Ck_2^4}{2\epsilon_2^{3/2}} Re\left[\int_0^\infty dv \frac{v}{(1 - v^2)^{1/2}} \times \left(\frac{\mu^2}{2} \{1 + r^s \exp[i2k_2 z(1 - v^2)^{1/2}]\} \right) \right] \quad \text{(A2)}$$

$$P_z(z) = \frac{ck_2^4}{2\epsilon_2^{3/2}} Re\left[\int_0^\infty dv \frac{v^3}{(1 - v^2)^{1/2}} \times (\mu^2 \{1 + r^p \exp[i2k_2 z(1 - v^2)^{1/2}]\}) \right] \quad \text{(A3)}$$

Equations A1–A3 were integrated numerically over the interval $v = 0$ to infinity. The integration was performed numerically in intervals (0 to 1, 1 to n_2/n_1, and/or n_2/n_1 to infinity), where the integrand is entirely real. Fig. 2 *A* shows results of a series of integrations for specified values of $z = 0$ to 3 μm.

In an ensemble of randomly oriented and distributed dipoles near a dielectric interface, each dipole will have a lifetime that depends upon its distance from the interface and its orientation with respect to the interface. Lifetimes for all orientations and distances must be included in a rigorous calculation of the single apparent lifetime observed for this distribution. To simplify this cumbersome calculation, average power dissipation (inverse of lifetime) was calculated with photoselection for all dipole orientations at each distance, z, from the interface (Eqs. A4–A6). Average power dissipation was then used to calculate phase angles and modulation ratios over z (Eqs. A7–A10). The rationale for this approximation is that polarized TIR illumination preferentially excites certain dipole orientations (photoselection), thus reducing the variance of the lifetime distribution at each z. Average relative power dissipation at z from randomly oriented dipoles excited by TIR illumination was approximated by

$$\langle P_x(z) \rangle = \int_0^{\pi/2} d\phi \int_0^{\pi/2} d\psi [P_x(z) \sin^4\psi \cos^2\phi \sin\phi + P_y(z) \sin^4\psi \cos^2\phi \sin\phi + P_z(z)\cos^2\psi \sin^2\psi \cos^2\phi \sin\phi] \quad \text{(A4)}$$

$$\langle P_y(z) \rangle = \int_0^{\pi/2} d\phi \int_0^{\pi/2} d\psi [P_x(z)\sin^4\psi \sin^2\phi \cos\phi + P_y(z)\sin^4\psi \cos^2\phi \sin\phi + P_z(z)\cos^2\psi \sin^2\phi \cos\phi] \quad \text{(A5)}$$

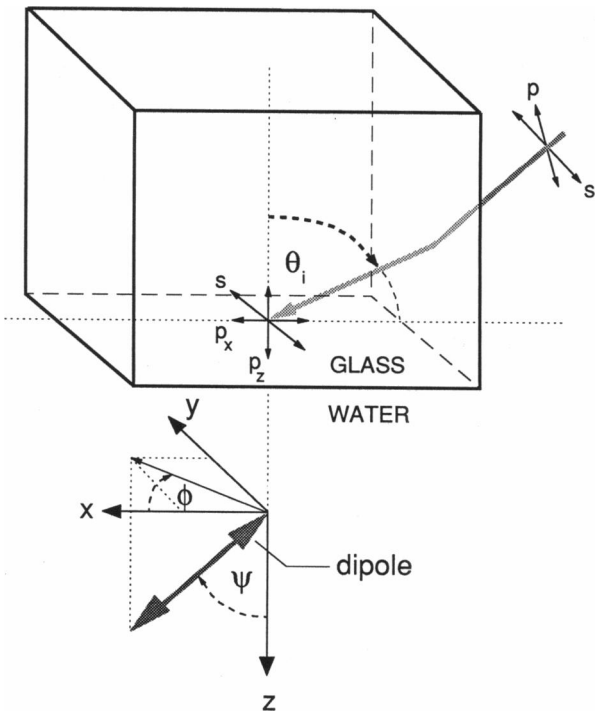

FIGURE 6 (Appendix) Definition of axes. The bottom surface of the glass-dielectric defines the x, y plane with positive z as the normal projecting into the aqueous region containing fluorophores. The incident plane is defined by the incident beam and the normal to the dielectric-aqueous interface. Trans and TIR evanescent field excitation are polarized perpendicular to the incident plane (s-polarized) with the electric vector along the y axis or polarized parallel to the incident plane (p-polarized) with an electric vector having x and z components. The angle of the incident beam is θ_i, and the orientation of a fluorophore is defined by the polar angle, ψ, and azimuthal angle, ϕ. See Appendix for details.

$$\langle P_z(z) \rangle = \int_0^{\pi/2} d\phi \int_0^{\pi/2} d\psi [P_x(z)\cos^2\psi \sin^3\psi + P_y(z)\cos^2\psi \sin^3\psi + P_z(z)\cos^4\psi \sin\psi] \quad \text{(A6)}$$

which combine functions for power dissipation from parallel ($P_x(z) \sin^2\psi$ and $P_y(z) \sin^2\psi$) and perpendicular ($P_z(z) \cos^2\psi$) dipoles with photoselection ($|\mu \cdot E_{ex}|$) by x, y, and z polarized excitation (see Results). These expressions were numerically integrated over ϕ and ψ for specified values of z. Fig. 2 *B* shows results of a series of integrations for $z = 0$ to 3 μm.

$N(\omega,\theta_i)$ and $D(\omega,\theta_i)$ were calculated by

$$N_s(\omega,\theta_i) = \int_0^\infty \frac{I_{0_y} e^{-z/d(\theta_i)} \omega[1/\langle P_y(z) \rangle]^2}{1 + \omega^2[1/\langle P_y(z) \rangle]^2} dz \quad \text{(A7)}$$

$$D_s(\omega,\theta_i) = \int_0^\infty \frac{I_{0_y} e^{-z/d(\theta_i)} [1/\langle P_y(z) \rangle]}{1 + \omega^2[1/\langle P_y(z) \rangle]^2} dz \quad \text{(A8)}$$

for s-polarized excitation and by

$$N_p(\omega,\theta_i) = \int_0^\infty \frac{I_{0_x} e^{-z/d(\theta_i)} \omega[1/\langle P_x(z) \rangle]^2}{1 + \omega^2[1/\langle P_x(z) \rangle]^2} + \frac{I_{0_z} e^{-z/d(\theta_i)} \omega[1/\langle P_z(z) \rangle]^2}{1 + \omega^2[1/\langle P_z(z) \rangle]^2} dz \quad \text{(A9)}$$

$$D_p(\omega,\theta_i) = \int_0^\infty \frac{I_{0_x} e^{-z/d(\theta_i)} [1/\langle P_x(z) \rangle]}{1 + \omega^2[1/\langle P_x(z) \rangle]^2} + \frac{I_{0_z} e^{-z/d(\theta_i)} [1/\langle P_z(z) \rangle]}{1 + \omega^2[1/\langle P_z(z) \rangle]^2} dz \quad \text{(A10)}$$

for p-polarized excitation. Initial intensity, I_0, of the x, y, and z polarized components of the evanescent field is given by,

$$I_{0_x} = J_p \frac{4\cos^2\theta_i(\sin^2\theta_i - n^2)}{n^4\cos^2\theta_i + \sin^2\theta_i - n^2} \quad \text{(A11)}$$

$$I_{0_y} = J_s \frac{4\cos^2\theta_i}{1 - n^2} \quad \text{(A12)}$$

$$I_{0_z} = J_p \frac{4\cos^2\theta_i \sin^2\theta_i}{n^4\cos^2\theta_i + \sin^2\theta_i - n^2} \quad \text{(A13)}$$

where J_s and J_p are the intensities of the incident s- and p-polarized light, and n (0.87) is the ratio of the refractive indices of the dielectric glass and aqueous medium (Axelrod, 1989). Equations A7–A10 were numerically integrated over z = 0–3 μm for 40 modulation frequencies (ω = 5–200 MHz). When the rotational correlation time is much shorter than the fluorescence lifetime, fluorophores photoselected by s- or p-polarized excitation will have randomized their orientation at the time of emission. Average power dissipation for randomized dipoles was calculated by integration of power dissipation for parallel and perpendicular dipoles without photoselection ($|\mu \cdot E_{ex}|$) at specified values of z as given by

$$\langle P_r(z)\rangle = \int_0^{\pi/2}\int_0^{\pi/2} \sin\psi\, d\psi [[P_x(z) + P_y(z)]\sin^2\psi + P_z(z)\cos^2\psi] \quad \text{(A14)}$$

$\langle P_r(z)\rangle$ was substituted for $\langle P_y(z)\rangle$ in Eqs. A7 and A8 to calculate $N(\omega,\theta_i)$ and $D(\omega,\theta_i)$. Phase angles and modulation ratios for frequency-domain fluorimetry measurements were calculated for values of ω as a function of θ_i (see text).

We thank Drs. Daniel Axelrod and Edward Hellen for extremely helpful advice and suggestions in the theory and practical setup of TIR fluorescence spectroscopy and Drs. James Abney and Bethe Scalettar for critical reading of the manuscript.

This work was supported by grants DK43840, DK16095, and DK35124 from the National Institutes of Health, a grant-in-aid from the American Heart Association, and a grant from the National Cystic Fibrosis Foundation. We are grateful for the donation of an argon laser and generous equipment support by the Engmann Family Foundation. We are also grateful for the use of an argon laser provided by Dr. Noel Warner and the Immunocytometry Division of the Becton-Dickinson Technical Corporation. Dr. Bicknese was supported in part by NRSA grant GM15145 from the National Institutes of Health. Dr. Verkman is an established investigator of the American Heart Association.

REFERENCES

Ausiello, D. A., J. Hartwig, and D. Brown. 1987. Membrane and microfilament organization and vasopressin action in transporting epithelia. *Soc. Gen. Physiol. Ser.* 42:259–275.

Axelrod, D. 1981. Cell-substrate contacts illuminated by total internal reflection fluorescence. *J. Cell Biol.* 89:141–145.

Axelrod, D. 1989. Total internal reflection fluorescence microscopy. *In* Methods in Cell Biology. Vol. 30. D. L. Taylor, and Y.-L. Wang, editors. Academic Press, New York. 245–270.

Axelrod, D., T. P. Burghardt, and N. L. Thompson. 1984. Total internal reflection fluorescence. *Annu. Rev. Biophys. Bioeng.* 13:247–268.

Born M., and E. Wolf. 1970. Principles of Optics. Pergamon Press, New York. 561–564.

Carniglia, C. K., L. Mandel, and K. H. Drexhage. 1972. Absorption and emission of evanescent photons. *J. Opt. Soc. Am.* 62:479–486.

Chance, R. R., A. Prock, and R. Silbey. 1978. Molecular fluorescence and energy transfer near interfaces. *Adv. Chem. Phys.* 37:1–65.

Chen, R. C., and C. H. Scott. 1985. Atlas of fluorescence spectra and lifetimes of dyes attached to protein. *Anal. Lett.* 18:393–421.

Clegg, J. S. 1984. Properties and metabolism of the aqueous cytoplasm and its boundaries. *Am. J. Physiol.* 246:R133–R151.

Dix, J. A., and A. S. Verkman. 1990. Mapping of fluorescence anisotropy in single cells by ratio imaging: application to cytoplasmic viscosity. *Biophys. J.* 57:231–240.

Drexhage, K. H. 1970. Influence of a dielectric interface on fluorescence decay time. *J. Lumin.* 12:693–701.

Fulton, A. B. 1982. How crowded is the cytoplasm? *Cell.* 30:345–347.

Fushimi, K., and A. S. Verkman. 1991. Low viscosity in the aqueous domain of cell cytoplasm measured by picosecond polarization microscopy. *J. Cell Biol.* 112:719–725.

Fushimi, K., J. A. Dix, and A. S. Verkman. 1990. Cell membrane fluidity in the intact kidney proximal tubule measured by orientation independent fluorescence anisotropy imaging. *Biophys. J.* 57:241–254.

Gingell, D., I. Todd, and J. Bailey. 1985. Topography of cell-glass apposition revealed by total internal reflection fluorescence of volume markers. *J. Cell Biol.* 100:1334–1338.

Gingell, D., O. S. Heavens, and J. S. Mellor. 1987. General electromagnetic theory of total internal reflection fluorescence: the quantitative basis for mapping cell-substratum topography. *J. Cell Sci.* 87:677–693.

Hlady, V. 1991. Spatially resolved adsorption kinetics of immunoglobulin G onto the wettability gradient surface. *Appl. Spectrosc.* 45:246–252.

Hellen, E. H., and D. Axelrod. 1987. Fluorescence emission at dielectric and metal-film interfaces. *J. Opt. Soc. Am. B* 4:337–350.

Kao, H. P., J. R. Abney, and A. S. Verkman. 1993. Determinants of the translational diffusion of a small solute in cell cytoplasm. *J. Cell Biol.* 120:175–184.

Lanni, F., A. S. Waggoner, and D. L. Taylor. 1985. Structural organization of interphase 3T3 fibroblasts studied by total internal reflection fluorescence microscopy. *J. Cell Biol.* 100:1091–1102.

Lepock, J. R., K. H. Cheng, S. D. Campbell, and J. Kruuv. 1983. Rotational diffusion of tempone in the cytoplasm of Chinese hamster lung cells. *Biophys. J.* 44:405–412.

Liebmann, L. W., J. A. R. Robinson, and K. G. Mann. 1991. A dual beam total internal reflection fluorescence spectrometer for dynamic depth resolved measurements of biochemical liquid-solid interface binding reactions in opaque solvents. *Rev. Sci. Instrum.* 62:2083–2092.

Luby-Phelps, K., D. L. Taylor, and F. Lanni. 1986. Probing the structure of cytoplasm. *J. Cell Biol.* 102:2015–2022.

Luby-Phelps, K., S. Mujundar, R. Mujundar, L. Ernst, W. Galbraith, and A. Waggoner. 1993. A novel fluorescence ratiometric method confirms the low solvent viscosity of the cytoplasm. *Biophys. J.* 65:236–242.

Lukosz, W., and R. E. Kunz. 1977. Fluorescence lifetime of magnetic and electric dipoles near a dielectric interface. *Optics Commun.* 20:195–199.

Mastro, A. M., and A. D. Keith. 1984. Diffusion in the aqueous compartment. *J. Cell Biol.* 99:180s-187s.

Masuhara, H., S. Tazuke, N. Tamai, and I. Yamazaki. 1986. Time-resolved total internal reflection fluorescence spectroscopy for surface photophysics studies. *J. Phys. Chem.* 90:5830–5835.

Periasamy, N., M. Armijo, and A. S. Verkman. 1991. Picosecond rotation of small polar fluorophores in the cytosol of sea urchin eggs. *Biochemistry.* 30:11836–11841.

Periasamy, N., H. P. Kao, and A. S. Verkman. 1992. Organic osmolytes increase cytoplasmic microviscosity in kidney cells. *Am. J. Physiol.* 263: C901–C907.

Parsegian, V. A., and D. C. Rau. 1984. Water near intracellular surfaces. *J. Cell Biol.* 99:196s-200s.

Porter, K. R. 1984. The cytomatrix: a short history of its study. *J. Cell Biol.* 99:3s-12s.

Reichert, W. M., and G. A. Truskey. 1990. Total internal reflection fluorescence (TIRF) microscopy: I. Modeling cell contact region fluorescence. 1990. *J. Cell Sci.* 96:219–230.

Suci, P., and V. Hlady. 1990. Fluorescence lifetime components of Texas Red-labeled bovine serum albumin: comparison of bulk and adsorbed states. *Colloids Surf.* 51:89–104.

Thompson, N. L., and T. P. Burghardt. 1986. Total internal reflection fluorescence: measurement of spatial and orientational distributions of fluorophores near planar dielectric interfaces. *Biophys. Chem.* 25:91–97.

Thompson, N. L., H. M. McConnell, and T. P. Burghardt. 1984. Order in

supported phospholipid monolayers detected by the dichroism of fluorescence excited with polarized evanescent illumination. *Biophys. J.* 46: 739–747.

Tilton, R. D., C. R. Robertson, and A. P. Gast. 1990. Lateral diffusion of bovine serum albumin. *Biophys. J.* 58:1321–1326.

Timbs, M. M., and N. L. Thompson. 1990. Slow rotational mobilities of antibodies and lipids associated with substrate-supported phospholipid monolayers as measured by polarized fluorescence photobleaching recovery. *Biophys. J.* 58:413–428.

Verkman, A. S. 1991. New microfluorimetry approaches to examine cell dynamics. *Comments Mol. Cell. Biophys.* 7:173–187.

Verkman, A. S., M. Armijo, and K. Fushimi. 1991. Construction and evaluation of a frequency-domain epifluorescence microscope for lifetime and anisotropy decay measurements in subcellular domains. *Biophys. Chem.* 40:117–125.

Weber, G. 1981. Resolution of the fluorescence lifetimes in heterogeneous system by phase and modulation measurements. *J. Phys. Chem.* 85:949–953.